European Journal of Mechanics / A Solids

A computational insight on damage-based constitutive modelling in femur mechanics

--Manuscript Draft--

Manuscript Number:	
Article Type:	Full Length Article
Keywords:	Femur biomechanics; Patient-specific finite-element modelling; Bone constitutive models; Damage mechanics; Bone failure criteria
Corresponding Author:	Pierfrancesco Gaziano ITALY
First Author:	Pierfrancesco Gaziano
Order of Authors:	Pierfrancesco Gaziano
	Cristina Falcinelli
	Giuseppe Vairo
Abstract:	The present paper addresses femur failure mechanics, by numerically investigating the influence of brittle/quasi-brittle bone constitutive description when combined with several failure criteria and different descriptions of bone ultimate parameters. Starting from computed tomography images of an experimentally-tested cadaveric femur, the bone geometry has been reconstructed through a semi-automatic segmentation procedure, and patient-specific material properties have been derived. Loading-induced loss of structural integrity has been simulated through a progressive damage model, by considering different damage evolution laws. An in-house displacement-driven incremental approach has been implemented in a finite element framework to mimic the in-vitro experimental procedure. Depending on the adopted modelling strategy, significant differences in terms of yield and failure load, as well as in fracture patterns, have been numerically experienced. Comparisons between the proposed numerical results and the available experimental outcomes have been carried out. In particular, for the femur model herein analyzed , elastic quasi-brittle bone descriptions combined with strain-based failure criteria seem to be more effective in predicting the mechanical behaviour up to the fracture.
Suggested Reviewers:	Cari Whyne cari.whyne@sunnybrook.ca She is an expert in femur features and modelling.
	Marcello Vasta Professor marcello.vasta@unich.it He is an expert in constitutive modelling of materials with application to tissue biomechanics.
	Stephane Avril avril@emse.fr He is an expert in computational methods and damage-based approaches for biological tissues.
	Alessio Gizzi a.gizzi@unicampus.it He is an expert in the constitutive modelling of biological tissues.

Prof. **Marc Geers**
Editor-in-Chief of
European Journal of Mechanics - A/Solids

Rome, 03 December 2021

Object: Manuscript submission

Dear Professor Geers,

Please find enclosed the manuscript entitled "*A computational insight on damage-based constitutive modelling in femur mechanics*", authored by Pierfrancesco Gaziano, Cristina Falcinelli and Giuseppe Vairo.

All authors acknowledge that:

- this manuscript is not submitted, nor published elsewhere;
- each Author has been involved in the study, and has read and approved the submitted version;
- there are no known conflicts of interest associated with this publication and there has been no financial support for this work that could have influenced its outcome.

We kindly ask you to consider this manuscript for publication in *European Journal of Mechanics – A/Solids*

Many thanks and best regards,

Pierfrancesco Gaziano
Cristina Falcinelli
Giuseppe Vairo

A computational insight on damage-based constitutive modelling in femur mechanics

Pierfrancesco Gaziano* [a], Cristina Falcinelli [b], Giuseppe Vairo [a]

[a] *Department of Civil Engineering & Computer Science (DICII), University of Rome "Tor Vergata", Via del Politecnico 1, 00133 Rome, Italy*

[b] *Department of Engineering and Geology (InGeo), G. DAnnunzio Chieti-Pescara University, Viale Pindaro 42, 65127 Pescara, Italy*

Abstract

The present paper addresses femur failure mechanics, by numerically investigating the influence of brittle/quasi-brittle bone constitutive description when combined with several failure criteria and different descriptions of bone ultimate parameters. Starting from computed tomography images of an experimentally-tested cadaveric femur, the bone geometry has been reconstructed through a semi-automatic segmentation procedure, and patient-specific material properties have been derived. Loading-induced loss of structural integrity has been simulated through a progressive damage model, by considering different damage evolution laws. An in-house displacement-driven incremental approach has been implemented in a finite element framework to mimic the in-vitro experimental procedure. Depending on the adopted modelling strategy, significant differences in terms of yield and failure load, as well as in fracture patterns, have been numerically experienced. Comparisons between the proposed numerical results and the available experimental outcomes have been carried out. In particular, for the femur model herein analyzed, elastic quasi-brittle bone descriptions combined with strain-based failure criteria seem to be more effective in predicting the mechanical behaviour up to the fracture.

Key words: Femur biomechanics, Patient-specific finite-element modelling, Bone constitutive models, Damage mechanics, Bone failure criteria

*Corresponding Author Email address: gaziano@ing.uniroma2.it (P. Gaziano).

1 Introduction

Over the last decades, femur fracture has become a topic of major concern, representing one of the main factors of morbidity, thus potentially jeopardising the patient's quality of life and leading in some cases to death [1, 2]. It has been estimated that in 2050 the

worldwide number of femur fractures, due exclusively to osteoporosis, will rise to more than 6 millions [3,4]. However, osteoporosis is just one of the possible factors that increase the femoral fracture risk, since other events, such as a fall or the presence of metastases, can induce a bone fracture [1,5–7]. In current clinical practice, the risk of femoral fracture is evaluated through some clinical parameters or indices, such as the areal bone mineral density in the case of osteoporosis and the Mirels' scoring system in the case of metastatic bones. Nevertheless, actual clinical standards suffer from a lack of specificity, resulting uneffective in a number of cases actually characterized by a high risk of fracture [8–12]. This limitation is essentially due to the fact that actual clinical assessment strategies disregard a number of subject-specific mechanical determinants, strictly related to specific loading characteristics, bone morphology, and dominant biomechanical features at both macro- and microscale [13].

Personalized finite-element (FE) modelling approaches, based on diagnostic imaging techniques, have been widely employed to investigate the mechanical behaviour of femurs, proving to be effective for tracing some quantitative and reliable estimates of femur fracture risk [8, 14–16]. Computed tomography (CT) has been frequently adopted as imaging technique allowing both to reconstruct the femur anatomical shape and to derive local values of bone mineral density [17–20]. The bone domain is subsequently discretized by using FE techniques, and a (usually) inhomogeneous distribution of bone material properties is deduced by combining the local values of bone density with experimental-based relationships [21–23].

Besides these common features, many differences exist among available FE modelling strategies. For instance, addressing the constitutive description, different material mapping strategies have been developed, which were proved to significantly affect the outcomes of CT-based FE femoral models [24]. In addition, several semi-empirical relationships associating local values of Young's modulus to local density of bone are available [21], as well as a number of constitutive models and strength criteria, differently combined for implementing numerical schemes, have been proposed for femur [18, 25–28]. Nevertheless, to the best of the authors' knowledge, there is a lack of conclusive indications for identifying the most effective and reliable modelling strategy [29]. As a matter of fact, many numerical studies addressing the mechanical response of femurs have highlighted values of the determination coefficient (R^2) ranging from 0.55 to 0.97, depending on the adopted modelling approach [24]. Such a wide range of R^2 proves that in many cases the model accuracy is sufficient, though not optimal.

In this framework, comparative analyses have been conveniently performed to trace more decisive conclusions regarding the effectiveness of certain modelling strategies over others.

The influence of the strength criterion on the FE prediction of femoral failure was examined both by Keyak & Rossi [25] and by Yosibash et al. [28]. In the combined numerical/experimental study performed by Keyak & Rossi stress-based theories were found to be more performing in predicting the femur failure, whereas Yosibash et al. demonstrated that strain-based criteria are more suitable for numerical predictions of bone-like mate-

rials, in agreement with other studies [30, 31]. As a consequence, definitive conclusions about the effectiveness of a criterion over another still cannot be traced.

As regards the constitutive modelling, Derikx et al. [32] numerically focused on the effects of the asymmetry in the bone strength parameters. In detail, the authors compared fracture patterns and failure loads obtained via Drucker-Prager strength criterion and (stress-based) Von Mises one, proving that the best predictions were achieved for the models based on Drucker-Prager criterion, which is able to discriminate different material strength levels in tension and in compression, as it is typical for bone. Accordingly, such an evidence suggests that accounting for asymmetric bone strength features is a mandatory issue to obtain reliable and effective numerical predictions. Furthermore, the combined experimental/numerical study performed by Keyak [26] and addressing a single-leg stance, highlighted that a non-linear modelling is able to improve the femoral failure load predictions with respect to a linearly-elastic one. Nevertheless, the global mechanical response therein obtained significantly deviates from the experimental one, since the bone post-yielding behaviour was assumed to be plastic with a piecewise linear description, whereas it has been demonstrated that bone usually exhibits a brittle or quasi-brittle behaviour, depending on the strain rate [33, 34].

Recently, advanced FE techniques have been employed to model the (quasi)-brittle behaviour of femur, thus managing to numerically predict the progressive fracturing process and to obtain more realistic fracture patterns. EXtended Finite Element Method (XFEM), which is based on the enrichment of mesh elements by means of additional degrees of freedom thus allowing to model the displacement discontinuity induced by fracture, was adopted for instance by Marco et al. [35], and Gustafsson et al. [18], demonstrating a moderate ability in predicting the fracture pattern compared to the experimental results. Hambli and coworkers [36–38] followed a different approach to model the fracture process of human femur, by applying the so-called Mechanical Property Degradation (MPD) technique Differently from XFEM, in the MPD a local degradation of material properties up to negligible values is enforced to simulate the removal of mesh elements that have failed. It is important to remark that MPD is not a purely numeric strategy to simulate fracture, but it can be set in a physical framework, since the degradation of material properties can be described by incorporating the continuum damage mechanics (CDM) theory within the constitutive modelling. Both techniques were proved to predict the femoral mechanical response as well as fracture patterns with a reasonable accuracy. However, as reported by Marco et al. [39], better results can be achieved with the MPD technique, since XFEM-based approaches predicted small fracture paths due to issues of numerical convergence, giving therefore useful indications only for the onset of femoral fracture mechanisms. It is worth observing that, in the previously-mentioned studies attempting to model the fracture process in femurs, comparative analyses aiming to investigate the effect of the constitutive modelling parameters on the femoral mechanical response have not been extensively conducted.

In view of previous considerations, it clearly appears that there is a lack of indications in terms of the predictive performance of CDM-based strategies as depending on the bone failure criterion and bone ultimate parameters. Accordingly, present paper aims to furnish a contribution in this context. Starting from available well-established experimental evidence published in [15] and shared by the research group directed by professor Z. Yosibash (Tel Aviv University, Israel), different femur computational models, implementing several stress- and strain-based failure criteria coupled with a CDM formulation, have been built up by means of a CT-based FE approach. In order to simulate femoral failure mechanisms, and in the framework of a displacement-controlled incremental approach, different strategies have been adopted for describing onset and evolution of the non-linear damage processes. Results obtained by FE analyses have been compared with in-vitro experimental outcomes in terms of fracture patterns, and both yield and failure loads, thus allowing to furnish useful though not conclusive indications about the influence of damage-based constitutive modelling, failure criteria and bone strength features on the prediction accuracy.

2 Materials and Methods

The mechanical behaviour of the left femur of a female donor (76 years old), provided by the Departments of Pathology and Orthopaedics of the Hadassah University Hospital in Jerusalem (Israel), has been investigated through a personalized FE-based approach. The femur was studied by Yosibash et al. in [15], both via experimental tests under one-leg stance configuration and via a computational approach based on a linearly-elastic patient-specific FE formulation.

2.1 Geometry reconstruction and meshing

In agreement with the experimental set-up, the computational domain was defined by referring to a femoral portion extending from the mid-diaphysis to the femoral head. To reconstruct the three-dimensional geometry, CT images (Fig. 1(a), corresponding scanning parameters are summarized in [15]), were segmented through a semi-automatic procedure by employing ITK-Snap software (v. 3.8, University of Pennsylvania, Philadelphia, PA). The segmentation procedure has been performed by accounting for operative indications provided by [40] in order to avoid partial volume effects, which could affect the stiffness mapping on the bone surface. The computational domain was discretized through 10-node displacement-based tetrahedral elements by using an automatic algorithm based on the Delaunay method within Comsol environment (Comsol with Matlab, v.5.4 COMSOL, Stockholm, Sweden). As a result of a preliminary convergence analysis, whose details are reported in Sec. 3.1, the average mesh size was set equal to $0.85 \cdot 10^{-2} H$ ($H = 230$ mm being the length of the analysed femoral portion, Fig. 1(b)). Accordingly, the computational model results in about 350000 elements and 1.5 millions degrees of freedom.

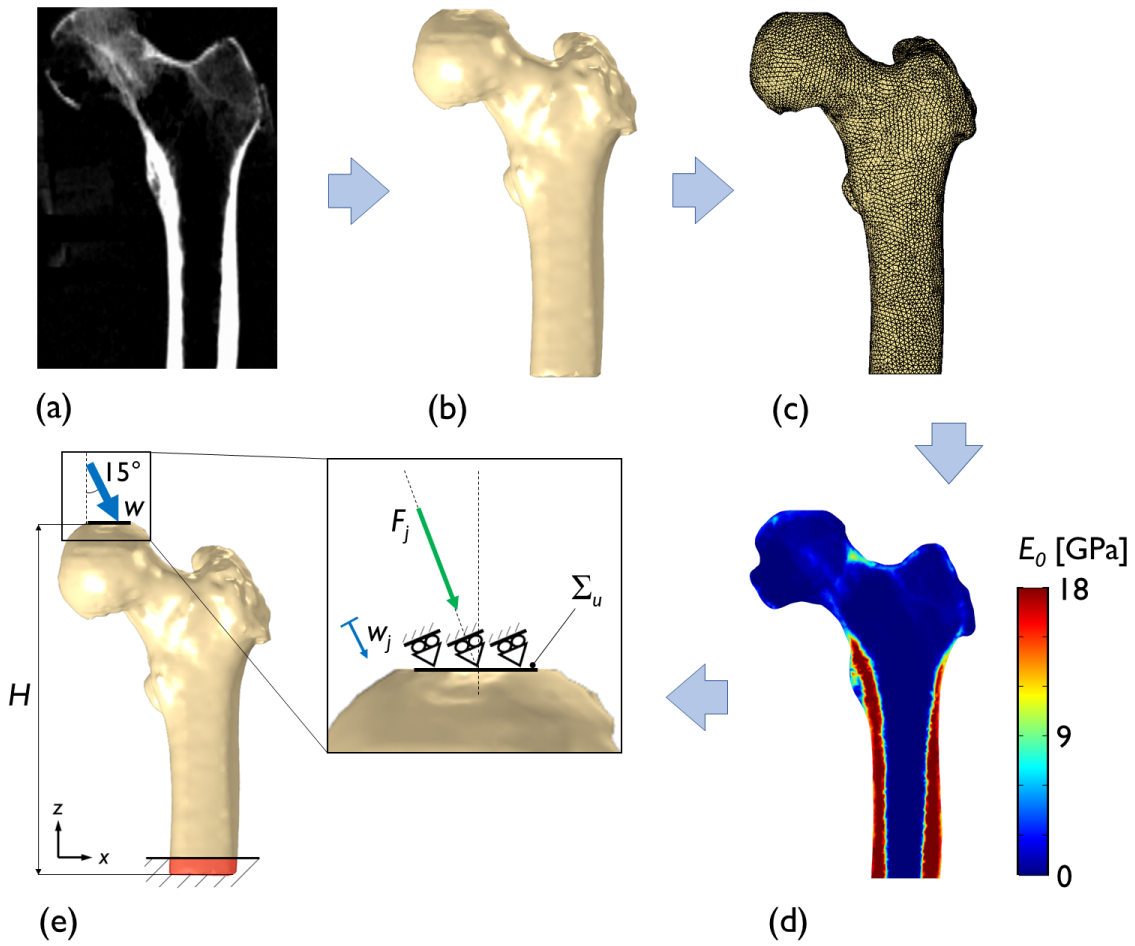

Fig. 1. CT-based FE modelling approach. CT scans (a) have been segmented to reconstruct the three-dimensional femur geometry (b) and the computational domain has been discretized using second-order tetrahedral elements (c). The heterogeneous distribution of the elastic modulus E_0 in the reference (i.e., undamaged) configuration has been computed from the density distribution derived from the CT images (d). A displacement-controlled loading path has been enforced at the femoral head with an orientation of 15° with respect to the diaphyseal axis (z-axis). The distal portion of the femoral model (4 mm long) has been fully restrained (e).

2.2 Constitutive modelling

2.2.1 CT-based subject-specific material properties

Femur has been assumed as a heterogeneous isotropic material. Any viscous and fluid effect has been disregarded, so that the local constitutive behaviour was completely described by local values of Young's modulus E and Poisson's ratio ν.

According to [41], Poisson's ratio has been assumed equal to $\nu = 0.3$ through the whole femur. Conversely, in agreement with a well-established modelling strategy [15, 16, 42, 43],

an heterogeneous Young's modulus distribution has been derived on the basis of the bone density distribution obtained from CT images. Specifically, the Hounsfield Unit (HU) value of each CT voxel was correlated to a local value of bone mineral density ρ_M through the empirical calibration equation reported in [15]:

$$\rho_M \ [\mathrm{g/cm^3}] = 10^{-3} \cdot (0.8072 \cdot HU - 1.6) \tag{1}$$

The ρ_M distribution has been subsequently converted into a distribution of ash density ρ_{ash} through the relationship furnished by Yosibash et al. [15] and based on the well-extablished experimental calibration proposed by [44]:

$$\rho_{ash} \ [\mathrm{g/cm^3}] = 0.877 \cdot 1.21 \cdot \rho_M + 0.08 \tag{2}$$

Following the evidence in [15], local values of bone ash density such that $\rho_{ash} \geq 0.486$ g/cm^3 (respectively, $\rho_{ash} < 0.486$ g/cm^3) are assumed to identify cortical (resp., trabecular) bone regions. Local values of Young's modulus in the reference (i.e., undamaged) configuration E_0 have been assumed to be associated to the ρ_{ash} distribution by means of the following density-elasticity relationship [15]:

$$E_0 \ [\mathrm{GPa}] = \begin{cases} 33.9\,\rho_{ash}^{2.20} & \text{if } \rho_{ash} \leq 0.3\,\mathrm{g/cm^3} \\ 2.398 & \text{if } 0.3\,\mathrm{g/cm^3} < \rho_{ash} < 0.486\,\mathrm{g/cm^3} \\ 10.2\,\rho_{ash}^{2.01} & \text{if } \rho_{ash} \geq 0.486\,\mathrm{g/cm^3} \end{cases} \tag{3}$$

The resulting distribution of E_0 is sketched in Fig. 1(d), where reference is made to a section in the coronal plane. It clearly appears the well-defined distribution of stiffness properties for cortical and trabecular regions, confirming the absence of significant partial volume effects.

2.2.2 Damage models

Aiming to model the (quasi)-brittle behaviour of femur, a modelling approach based on the CDM theory has been adopted. Accordingly, the progressive loss of material integrity is locally described through a damage variable which, under the herein-assumed hypothesis of isotropic damage, is a scalar [45]. The damage variable, denoted with D in the following, is such that $D \in [0, D_{cr}]$, where the value $D = 0$ identifies a completely undamaged state and $D_{cr} \in (0, 1]$ is the critical value of D associated with a complete local failure [46,47]. Following the Lemaitre-Chaboche 3D elastic damage model [47], the linear elastic constitutive law can be recast as:

$$\boldsymbol{\sigma} = (1 - D)\,\mathbb{C}_0 : \boldsymbol{\varepsilon} \tag{4}$$

where $\boldsymbol{\sigma}$ is the second-order Cauchy stress tensor, $\boldsymbol{\varepsilon}$ is the second-order infinitesimal strain tensor and $\mathbb{C}_0$ is the fourth-order elasticity tensor of the undamaged material, satisfying minor and major symmetries and herein assumed to be dependent on E_0 and ν. Equation (4) shows that the growth of the damage variable corresponds to a reduction of the material stiffness, and therefore of its local load-carrying capacity.

Continuum damage models can be formulated either in strain or in stress space [46]. As a notation rule, in the following symbol $\eta \in \{\varepsilon, \sigma\}$ will be employed to generically denote a strain- or stress-related quantity. Moreover, for distinguishing the corresponding governing equations, subscripts ε and σ will be employed for strain and stress-based formulations, respectively.

Let κ_η be a non-negative internal variable, describing the maximum level of strain or stress locally attained during a loading process up to the actual state, this latter discriminated by a time-like variable t:

$$\kappa_\eta = \kappa_\eta(t) = \max\{\eta_0, \max_{\tau \leq t}\{\eta_{eq}(\tau)\}\} \tag{5}$$

where η_0 is a positive threshold (strain or stress) value at which the damage process triggers, and $\eta_{eq} = \eta_{eq}(t)$ is an equivalent positive (strain or stress) measure of the local strain or stress state $\boldsymbol{\eta} = \boldsymbol{\eta}(t)$ defined on the basis of a given strength criterion. Then, damage occurrence can be associated to the vanishing of a non-positive loading function g_η defined as:

$$g_\eta(\boldsymbol{\eta}, \kappa_\eta) = \eta_{eq}(\boldsymbol{\eta}) - \kappa_\eta \tag{6}$$

and damage description associated to loading/unloading processes can be formulated through an evolutive approach based on the Kuhn-Tucker relationships [46]:

$$\dot{\kappa}_\eta \geq 0, \qquad g_\eta \leq 0, \qquad \dot{\kappa}_\eta g_\eta = 0 \tag{7}$$

where the overdot denotes the derivative with respect to the time-like variable t. In particular, Eqs. (7) imply that damage evolves (i.e., $\dot{\kappa}_\eta > 0$) only if $g_\eta = 0$. Previous relationships have to be completed by choosing a suitable strength criterion (defining η_{eq}) and by assigning a damage evolution law $D = D(\kappa_\eta)$. This latter allows to evaluate damage accumulation during the loading path and it has to satisfy, as a thermodynamic consistency requirement, that D has to be a non-decreasing monotonic function with respect to t, due to the dissipative nature of damage mechanisms.

To account for the material constitutive asymmetry in tension and in compression, damage accumulation associated to a triaxal state is distinguished by referring to the sign of the first stress invariant $I_1 = \mathrm{tr}(\boldsymbol{\sigma})$. In particular, when $I_1 \geq 0$ (resp., when $I_1 < 0$), damage evolution is described by the damage variable $D^+ = D^+(\kappa_\eta^+)$ and by the loading function g_η^+, defined in terms of the internal variable κ_η^+ and of the positive threshold value η_0^+ (resp., by the damage variable $D^- = D^-(\kappa_\eta^-)$ and by the loading function g_η^-, defined in

terms of the internal variable κ_η^- and of the positive threshold value η_0^-). The damage variable D, accounting for a generic loading history, is assumed to be described by:

$$D = D(t) = \frac{D^+ D_{cr}^+ (D_{cr}^- - D^-) + D^- D_{cr}^- (D_{cr}^+ - D^+)}{D_{cr}^+ D_{cr}^- - D^+ D^-} \tag{8}$$

D_{cr}^+ and D_{cr}^- being the critical value of D^+ and D^-, respectively. It is worth noting that for monotonic tensile (resp., compressive) loading conditions, D reads as D^+ (resp., D^-), and that when bone exhibits local failure under a tensile-like (resp., compressive-like) state, D reaches the limit value D_{cr}^+ (resp., D_{cr}^-). When this latter situation occurs, κ_η^+ (resp., κ_η^-) assumes the positive value η_f^+ (resp., η_f^-) representative of the bone (strain or stress) ultimate parameter in tension (resp., in compression).

In order to analyze the corresponding influence on the predicted mechanical behaviour of femur under single-leg stance loading conditions, bone damage-based constitutive response has been modelled by considering: different damage evolution laws, different descriptions of bone ultimate parameters, and different strain- or stress-based strength criteria. The various aspects investigated are detailed in Sections 2.2.3, 2.2.4 and 2.2.5.

2.2.3 Damage evolution laws

As regards the damage evolution laws, the mechanical behaviour of femur has been locally described by adopting either an elastic quasi-brittle or brittle constitutive response, respectively characterized by the presence or absence of a local gradual damage accumulation prior to failure. In what follows, the elastic quasi-brittle and brittle models will be labelled as EQB and EB models, respectively. In particular, both EQB and EB behaviours can be described through either a strain or stress-based formulation, as detailed below.

- **Strain-based elastic brittle model**
  In this case, the damage evolution law can be deduced in a simple form by relating the actual value of the damage variable D with the current value of the internal variable κ_ε (see Eq. (5)) as follows:

$$D^\pm = \begin{cases} 0 & \text{if } \kappa_\varepsilon^\pm < \varepsilon_f^\pm \\ D_{cr}^\pm & \text{if } \kappa_\varepsilon^\pm \geq \varepsilon_f^\pm \end{cases} \tag{9}$$

- **Stress-based elastic brittle model**
  Similarly to Eq. (9), the damage evolution law describing a stress-based elastic brittle response of bone can be straight deduced as:

$$D^\pm = \begin{cases} 0 & \text{if } \kappa_\sigma^\pm < \sigma_f^\pm \\ D_{cr}^\pm & \text{if } \kappa_\sigma^\pm = \sigma_f^\pm \end{cases} \tag{10}$$

- **Strain-based elastic quasi-brittle model**
  A phenomenological-based form of the damage law, relating the actual value of the

damage variable with the current values of $\kappa_\varepsilon^\pm$, has been adopted. Accordingly, in agreement with [36], the evolution of D (see Eq. (8)) has been locally described, discriminating tensile and compressive features, by the following relationship based on the experimental data provided in [48]:

$$D^\pm = \begin{cases} 0 & \text{if } \kappa_\varepsilon^\pm < \varepsilon_0^\pm \\ D_{cr}^\pm \left(\frac{\kappa_\varepsilon^\pm}{\varepsilon_f^\pm} \right)^{n_\varepsilon^\pm} & \text{if } \varepsilon_0^\pm \leq \kappa_\varepsilon^\pm < \varepsilon_f^\pm \\ D_{cr}^\pm & \text{if } \kappa_\varepsilon^\pm \geq \varepsilon_f^\pm \end{cases} \tag{11}$$

where $n_\varepsilon^\pm$ represents the damage-law exponent. According to [37], the values $n_\varepsilon^+ = n_\varepsilon^- = 2$ and $\varepsilon_0^+ = \varepsilon_0^- = 0.002$ have been herein assumed. It should be noted that the strain-based EB model is straight recovered by letting $n_\varepsilon^\pm \to +\infty$ in Eq. (11).

- **Stress-based elastic quasi-brittle model**

To the best of the authors' knowledge, a stress-based damage evolution law concerning bone tissue does not exist in literature. In order to account for a strain-softening phase, the evolution of the damage variable D is assumed to be regulated by a similar relationship as in Eq. (11), formulated in terms of a stress-based approach and thereby depending on σ_{eq} and $\kappa_\sigma^\pm$. In detail, the evolution of D (see Eq. (8)) has been locally described, discriminating tensile and compressive features, by:

$$D^\pm = \begin{cases} 0 & \text{if } \kappa_\sigma^\pm < \sigma_0^\pm \\ D_{cr}^\pm \left(\frac{\hat{\varepsilon}}{\hat{\varepsilon}_f^\pm} \right)^{n_\sigma^\pm} & \text{if } \sigma_0^\pm \leq \kappa_\sigma^\pm < \sigma_f^\pm \text{ and } \hat{\varepsilon} < \hat{\varepsilon}_M^\pm \\ D_{cr}^\pm \left(\frac{\hat{\varepsilon}}{\hat{\varepsilon}_f^\pm} \right)^{n_\sigma^\pm} & \text{if } \kappa_\sigma^\pm = \sigma_f^\pm \text{ and } \hat{\varepsilon}_M^\pm \leq \hat{\varepsilon} < \hat{\varepsilon}_f^\pm \\ D_{cr}^\pm & \text{if } \kappa_\sigma^\pm = \sigma_f^\pm \text{ and } \hat{\varepsilon} \geq \hat{\varepsilon}_f^\pm \end{cases} \tag{12}$$

where:

- the values of the damage law exponents $n_\sigma^+ = n_\sigma^- = 2$ have been herein employed, due to the lack of experimental evidence; nevertheless, a sensitivity analysis with respect to this modelling parameter has been performed and corresponding results are presented and discussed in Sec. 3.3;
- the values $\sigma_0^\pm = E_0 \varepsilon_0^\pm$ have been assumed owing to the linearity of the constitutive law up to the triggering of local damage process;
- $\hat{\varepsilon} = \hat{\varepsilon}(\sigma_{eq})$ denotes a positive strain measure associated to the equivalent stress one, assumed such that it satisfies the following relationship:

$$\sigma_{eq} = (1 - D) E_0 \hat{\varepsilon} \tag{13}$$

- $\hat{\varepsilon}_M^\pm = \hat{\varepsilon}_M^\pm(\sigma_f^\pm)$ is the strain measure attained when the equivalent stress measure reaches its maximum value, i.e. $\sigma_{eq} = \sigma_f^\pm$:

$$\hat{\varepsilon}_M^\pm = \left(1 + \frac{1}{n_\sigma^\pm} \right) \frac{\sigma_f^\pm}{E_0} \tag{14}$$

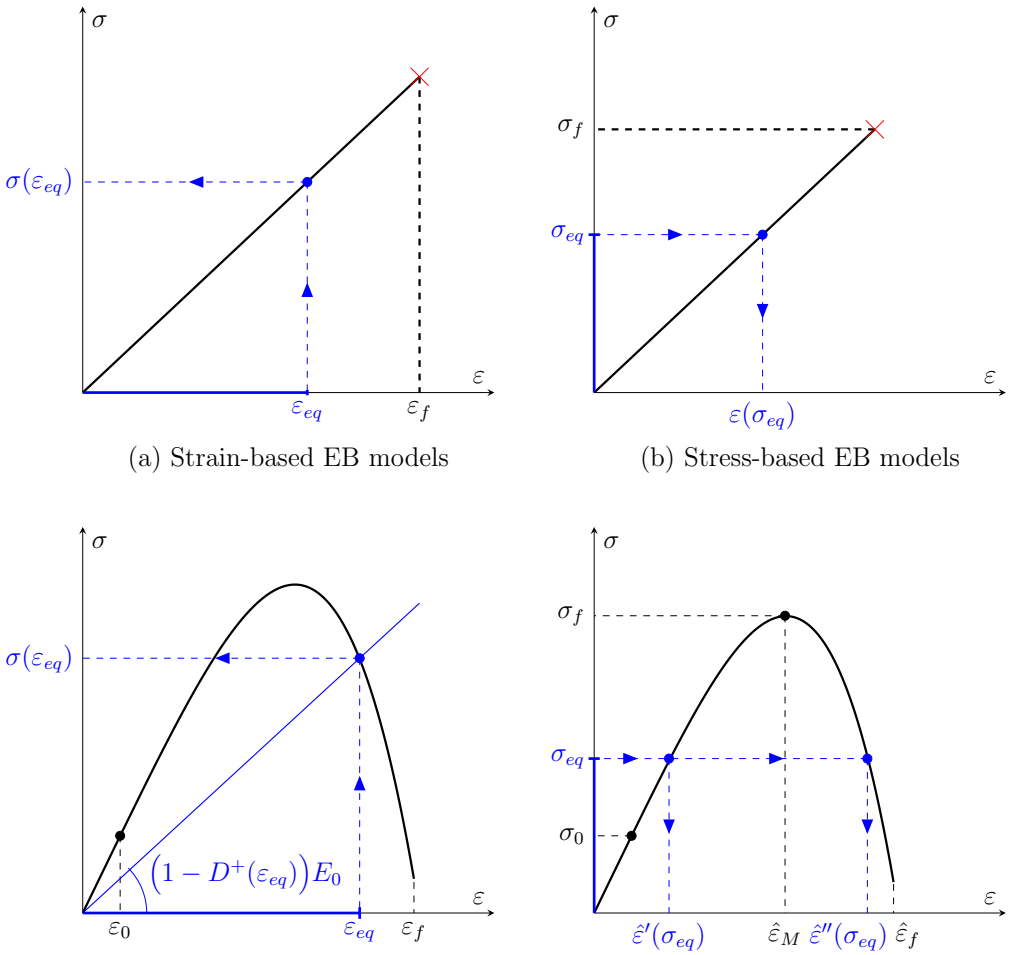

(a) Strain-based EB models (b) Stress-based EB models

(c) Strain-based EQB models (d) Stress-based EQB models

Fig. 2. Typical stress-strain curves representative of the different constitutive description herein employed. The notation has been introduced in Section 2.2.3.

- $\hat{\varepsilon}_f^{\pm} = \hat{\varepsilon}_f^{\pm}(\sigma_f^{\pm})$ is the stress-based measure of the failure strain, determined by enforcing that $d\sigma_{eq}/d\hat{\varepsilon} = 0$ when $\sigma_{eq} = \sigma_f^{\pm}$ (see Eq. (13)):

$$\hat{\varepsilon}_f^{\pm} = \left(D_{cr}^{\pm}\left(n_\sigma^{\pm}+1\right)\right)^{\frac{1}{n_\sigma^{\pm}}} \hat{\varepsilon}_M^{\pm} \tag{15}$$

It is worth observing that, since in this case $D = D(\hat{\varepsilon})$, the evaluation of $\hat{\varepsilon} = \hat{\varepsilon}(\sigma_{eq})$ by Eq. (13) can be performed by recurring to a numerical iterative procedure.

Figure 2 schematically illustrates the typical stress-strain curves corresponding to the four constitutive descriptions introduced above.

Table 1
Experimental-based values of bone ultimate parameters for strain-based models (PD models: description of bone ultimate strain via a piecewise-constant dependence on bone local density [37, 49]; CD models: description of bone ultimate strain via a continuous dependence on bone local density [50]).

	PD models		CD models
	Cortical	Trabecular	
ε_f^+ [–]	0.0157	0.0250	$0.0081\,\rho_{ash}^{-1.42}$
ε_f^- [–]	0.0250	0.0400	$0.0081\,\rho_{ash}^{-1.42}$

Table 2
Experimental-based values of bone ultimate parameters for stress-based models (PD models: description of bone ultimate stress via a piecewise-constant dependence on bone local density [22, 23]; CD models: description of bone ultimate stress via a continuous dependence on bone local density [28, 42, 51, 52]).

	PD models		CD models
	Cortical	Trabecular	
σ_f^+ [MPa]	91.60	6.17	$0.8\,\sigma_f^-$
σ_f^- [MPa]	131.50	7.71	$\begin{cases} 137\,\rho_{ash}^{1.88} & \text{if } \rho_{ash} \leq 0.317\,\text{g/cm}^3 \\ 114\,\rho_{ash}^{1.72} & \text{if } \rho_{ash} > 0.317\,\text{g/cm}^3 \end{cases}$

2.2.4 Bone ultimate parameters

With reference to experimental-based data available in the literature, bone ultimate parameters $\varepsilon_f^{\pm}$, $\sigma_f^{\pm}$ have been assumed to be either piecewise-constant or continuous functions of the local bone ash density. For the sake of conciseness, the corresponding models will be henceforth labelled as PD and CD models, respectively. Values and expression adopted in this work are reported in Tables 1 and 2 for $\varepsilon_f^{\pm}$ and $\sigma_f^{\pm}$, respectively. It is important to observe that a PD description of bone ultimate parameters allows to clearly distinguish trabecular and cortical tissue properties, as well as tensile and compressive limit states.

2.2.5 Equivalent strain and stress measures

Previous damage models have been coupled with both strain- and stress-based strength criteria.

- **Strain-based strength criteria**

  - *Maximum Principal Strain* (MPε). By denoting with ε_1, ε_2 and ε_3 the local principal strains, the equivalent strain measure is given by:

$$\varepsilon_{eq}^{(\mathrm{MP}\varepsilon)} = \begin{cases} \max\{0, \varepsilon_1, \varepsilon_2, \varepsilon_3\} & \text{in tension} \\ -\min\{0, \varepsilon_1, \varepsilon_2, \varepsilon_3\} & \text{in compression} \end{cases} \tag{16}$$

  - *Von Mises Strain* (VMε). According to [37], the following equivalent measure for the local strain state is adopted:

$$\varepsilon_{eq}^{(\mathrm{VM}\varepsilon)} = \sqrt{\frac{2}{3}\boldsymbol{\varepsilon}^{dev} : \boldsymbol{\varepsilon}^{dev}} \tag{17}$$

  where $\boldsymbol{\varepsilon}^{dev}$ represents the deviatoric part of the strain tensor.

- **Stress-based strength criteria**

  - *Maximum Principal Stress* (MPσ). By denoting with σ_1, σ_2 and σ_3 the local principal stresses, the equivalent stress measure is given by:

$$\sigma_{eq}^{(\mathrm{MP}\sigma)} = \begin{cases} \max\{0, \sigma_1, \sigma_2, \sigma_3\} & \text{in tension} \\ -\min\{0, \sigma_1, \sigma_2, \sigma_3\} & \text{in compression} \end{cases} \tag{18}$$

  - *Von Mises stress* (VMσ). In this case, the equivalent stress measure $\sigma_{eq}^{(\mathrm{VM})}$ is evaluated as:

$$\sigma^{(\mathrm{VM})} = \sqrt{\frac{3}{2}\boldsymbol{\sigma}^{dev} : \boldsymbol{\sigma}^{dev}} = \sqrt{3I_2^{dev}} \tag{19}$$

  where $\boldsymbol{\sigma}^{dev}$ and I_2^{dev} represent the deviatoric stress tensor and its second invariant, respectively.

  - *Drucker-Prager stress* (DPσ). According to [27], the Drucker-Prager equivalent stress $\sigma_{eq}^{(\mathrm{DP})}$ is given by:

$$\sigma_{eq}^{(\mathrm{DP}\sigma)} = \sqrt{3}\left(\alpha I_1 + \sqrt{I_2^{dev}}\right) \tag{20}$$

  where α is a material parameter associated to an asymmetric constitutive response in tension/compression and expressed as [53]:

$$\alpha = \frac{1}{\sqrt{3}}\frac{\sigma_f^- - \sigma_f^+}{\sigma_f^- + 2\sigma_f^+} \tag{21}$$

  It is worth noting that $\sigma_{eq}^{(\mathrm{DP}\sigma)} \to \sigma_{eq}^{(\mathrm{VM}\sigma)}$ when $\alpha \to 0$, resulting in this case in a symmetric tension/compression behaviour.

2.3 Numerical treatment

2.3.1 Boundary conditions

To reproduce the experimental procedure adopted in [15], numerical simulations have been implemented following a quasi-static displacement-controlled incremental approach. Specifically, with reference to the Fig. 1(e), incremental displacements have been enforced at the femoral head (by considering a pseudo-circular region Σ_u, 10 mm in diameter) with an orientation of 15 degrees with respect to the diaphyseal axis (z-axis) and following a monotonically increasing path. Moreover, a small portion of the external surface associated to the distal part of the mid diaphysis (4 mm long) has been fully restrained.

2.3.2 Regularization for mesh-sensitivity reduction

In order to obtain numerical results that are practically independent from the mesh size and then objective, a suitable regularization technique has been implemented by introducing the internal length λ related to the internal (heterogeneous) microstructure. As a matter of fact, for (quasi-)brittle materials the bandwidth of the localization zone of strains (and consequently the damage) can be considered to be a characteristic constitutive property of the material [54]. Accordingly, following the approach proposed in [55], a regularization method, based on a mesh-related local modification of material properties, has been adopted. Such a regularization approach results very effective, although its implementation is relatively more straightforward than other modelling strategies adopted in tissue biomechanics, which are often based on non-local damage formulations (see e.g. [56, 57]). Specifically, the experimental-based values of the bone ultimate parameters $\eta_f^{\pm}$ are corrected under the constraint that the dissipated energy per unit crack surface U_d equals the corresponding energy in the discretized model.

For every damage model introduced in Sec. 2.2.3, it can be proved that U_d is quadratic with respect to the ultimate parameter $\eta_f^{\pm}$, namely $U_d = O(\lambda\,\eta_f^2)$. In fact, let the uniaxial tensile behaviour of strain-based EQB models under a monotonic loading path be considered (the same discussion can be made for the compressive behaviour as well). By recalling Eqs. (4) and (11), and by omitting the superscript + for the sake of compactness, the dissipated unit-crack-surface energy U_d can be written as follows [55]:

$$\begin{aligned} U_d &= \lambda \int_0^{\varepsilon_f} \sigma d\varepsilon = \frac{1}{2}\lambda\, E_0\, \varepsilon_0^2 + \lambda \int_{\varepsilon_0}^{\varepsilon_f} \left[1 - D_{cr}\left(\frac{\varepsilon}{\varepsilon_f}\right)^{n_\varepsilon}\right] E_0 \varepsilon\, d\varepsilon \\ &= \frac{1}{2}\lambda E_0 \varepsilon_f^2 \left[1 - \frac{2D_{cr}}{n_\varepsilon + 2}\left(1 - \left(\frac{\varepsilon_0}{\varepsilon_f}\right)^{n_\varepsilon+2}\right)\right] \\ &\simeq \frac{1}{2}\lambda E_0 \varepsilon_f^2 \left(1 - \frac{2D_{cr}}{n_\varepsilon + 2}\right) \end{aligned} \tag{22}$$

resulting $(\varepsilon_0/\varepsilon_f)^{n_\varepsilon+2} \ll 1$, since $n_\varepsilon > 0$ and $\varepsilon_f \gg \varepsilon_0$. Thereby, it is straight deduced that

$U_d = O(\lambda\,\varepsilon_f^2)$.

It is worth noting that the same conclusion can be drawn for all the other damage laws presented in Sec. 2.2.3, since:

- the dissipated energy U_d for the stress-based EQB models can be evaluated as above, so long as ε_f is replaced by $\hat{\varepsilon}_f$;
- the strain-based EB models are recovered from the corresponding EQB models in the limit as $n_\varepsilon \to +\infty$;
- for the stress-based EB models, $\sigma_f = E_0\varepsilon_f$, and therefore one has $U_d = \lambda\sigma_f^2/(2E_0)$;

As a consequence, following a rationale analogous to the one proposed in [55], the experimentally obtained ultimate parameters $\eta_f^\pm$ are replaced for numerical applications and for each element by the corresponding corrected values:

$$\eta_{f,\,\mathrm{FE}}^\pm = \sqrt{\frac{\lambda}{h_e}}\,\eta_f^\pm \tag{23}$$

where h_e is the element characteristic dimension related to the local mesh size, and defined as: $h_e = \sqrt[3]{V_e}$, V_e being the element volume in the actual configuration.

In the following, in agreement with [58], the characteristic length λ associated to the femoral bone microstructure is assumed homogeneous and equal to 1.0 mm.

2.3.3 Iterative algorithm

To simulate a progressive damage process, a numerical iterative procedure has been developed in Matlab environment (Matlab, MathWorks, MA, USA) through home-made codes integrated within the commercial FE solver Comsol Multiphysics. Numerical simulations have been run on a multiprocessor Intel Xeon II HPZ800 workstation with 64 GB of RAM, requiring averagely 4 hours of computation time per simulation.

Starting from the discretized femoral model in the reference configuration, the undamaged constitutive properties have been locally assigned. Displacement increments equal to $\Delta w = 0.05$ mm have been considered, so that at the j-th computational step, the linearly-elastic problem associated to the actual secant constitutive response (see Eq. (4)) is solved by considering the enforced displacement value $w_j = j\Delta w$ (see Fig. 1).

After the solution of the linearly-elastic problem, the actual volume value of each element V_e is evaluated by multiplying the element volume in the reference configuration by the determinant of the local deformation gradient (i.e., the element Jacobian). Furthermore, possible increase of the local damage variable D is verified in agreement with the selected damage description (see Section 2.2.3) and strength criterion (see Section 2.2.5). If no damage increment is experienced within the overall computational domain, the force F_j

required to apply the prescribed displacement at j-th step is computed by numerically integrating the nodal reactive forces on Σ_u, and the subsequent computational step $j+1$ is carried out. On the contrary, if damage increase is detected somewhere in the computational domain, the corresponding local constitutive properties are degraded by locally enforcing that $E = (1 - D)E_0$. In addition, the j-th step is repeated until no further variations of the damage pattern is revealed (namely, no further elements are detected to fail), thus ensuring equilibrium and compatibility of the solution.

Local failure conditions, i.e. the crack initiation and propagation, are numerically detected by comparing the local actual value of D with critical values D_{cr}^{+} and D_{cr}^{-}, discriminating tensile-like or compressive-like local states. Specifically, in agreement with [36, 59], the value $D_{cr}^{+} = 0.95$ has been adopted for the critical damage in tension, as representative of a practically full loss of local material stiffness. On the other hand, failure in a compressive-like state is assumed to occur when $D_{cr}^{-} = 0.5$, to account for a non-negligible local stiffness possibly induced by self-contact/friction conditions between material sides. A sensitivity analysis on D_{cr}^{+} and D_{cr}^{-} with respect to a strain-based quasi-brittle damage model is available in [36].

2.3.4 Post-processing

By adopting the previously described approach, the complete load-displacement path, as well as the evolution of the damage pattern, have been detected. The maximum value of the force F_j recorded during the numerical simulations has been considered as representative of the femoral failure load. Moreover, following [15,28], the load at which a 5% slope variation is noticed with respect to the initial linear branch of the load-displacement curve has been evaluated and referred to as yield load. As a notation rule, failure and yield loads will be henceforth denoted with FL and YL, respectively. Finally, the fracture patterns associated to the different models have been defined by identifying the computational region where critical damage has been attained.

3 Results

3.1 Preliminary results: convergence of the solution upon mesh refinements

In order to validate the regularization technique described in Sec. 2.3.2, the biomechanical response of femur herein considered has been numerically investigated by employing three different mesh sizes (see Fig. 3(a)). For the sake of brevity, in the following results relevant to the EQB-PD model based on the Von Mises equivalent strain only have been reported. Simulations relevant to the other computational models herein defined show similar responses. In detail, an average element size equal to $1.75 \times 10^{-2}\, H$, $0.85 \times 10^{-2}\, H$ and $0.43 \times 10^{-2}\, H$ has been adopted for the coarse, average and fine mesh, respectively.

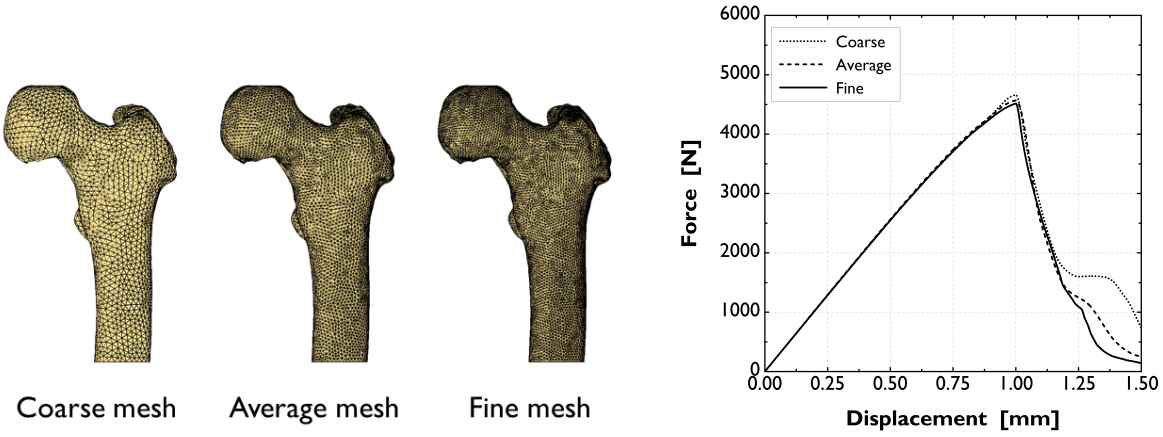

(a) (b)

Fig. 3. Preliminary mesh convergence analysis. (a) Discretization levels adopted, and (b) the corresponding force-displacement numerical predictions.

Panel in Fig. 3(b) reports the numerically-experienced mechanical response in terms of force-displacement curves for the three meshes. The FE-obtained curves clearly prove the effectiveness of the regularization approach presented in the foregoing. Accordingly, as a right balance between model accuracy and computational cost, the subsequent comparative analyses has been carried out by employing the average mesh.

3.2 FE-based comparative analysis

In the following, obtained numerical results are reported and compared to the experimental findings available in [15]. In detail, the influence of the coupling among damage-based constitutive modelling, failure criteria and bone strength features is addressed.

Figure 4 depicts the numerically-experienced load-displacement curves compared to the experimental one available from in-vitro mechanical tests [15]. Proposed results refer to quasi-brittle (EQB) and brittle (EB) models, defined in terms of the strain-based and stress-based criteria described in Section 2.2.5, and coupled with either a piecewise-constant (PD) or a continuous (CD) dependence of the bone ultimate parameters $\varepsilon_f^{\pm}$, $\sigma_f^{\pm}$ on the ash density (see Section 2.2.4). Correspondingly, Tables 3 and 4 summarize, respectively, the values of the yield load (YL) and of the failure load (FL) computed via the different modelling approaches herein considered, in comparison with available experimental data [15]. Values reported in brackets represent the absolute value of the relative error between the experimentally- and numerically-obtained values. Table 4 indicates also the corresponding failure mechanisms deduced by the numerically-predicted damage patterns. Exemplary damage patterns computed for a boundary displacement at the top of the femoral head equal to 2.5 mm are depicted in Figs. 5 and 6, by distinguishing strain- and stress-based criteria, respectively.

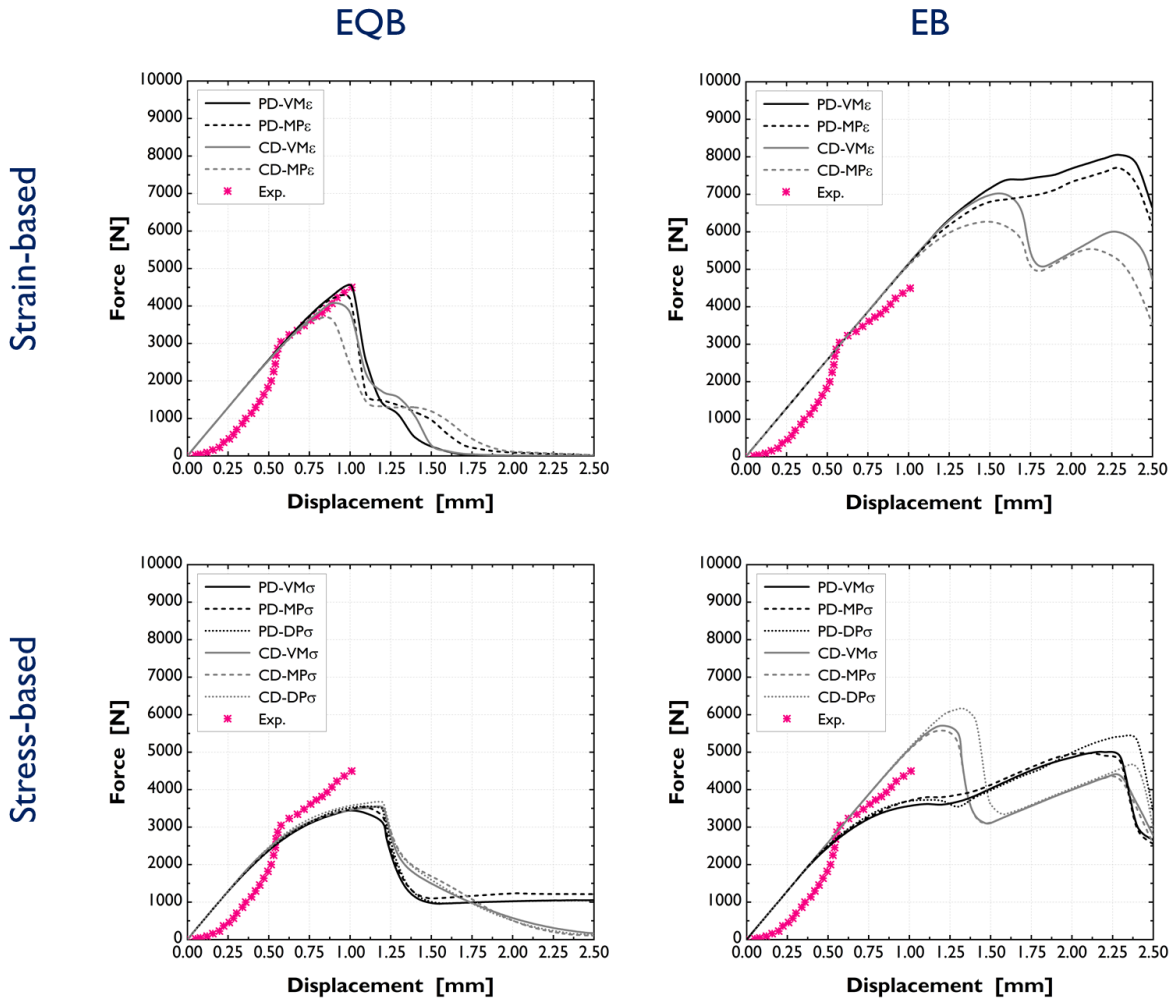

Fig. 4. Force-displacement curves numerically computed by considering different models. The first row (respectively, the second row) refers to strain-based (resp., stress-based) models, by distinguishing quasi-brittle (EQB, the first column) and brittle (EB, the second column) descriptions and addressing the strength criteria introduced in Section 2.2.5. PD (resp., CD): Piecewise-constant (resp., continuous) dependence of bone ultimate parameters on the density. Exp.: experimental data available in [15].

Figures 7 and 8 report the distributions at the coronal section of the Von Mises stress measure associated to suitable boundary displacement levels at the top of the femoral head inducing damaged states. In detail, Fig. 7 refers to the strain-based criteria and Fig. 8 to the stress-based ones.

3.3 Sensitivity analysis to the stress-based damage law exponent

The stress-based EQB model introduces new parameters such as the damage law exponents n_σ^+ and n_σ^- which are supposed to influence the results. Due to the uncertainty concerning the values of such parameters, arising from a lack of experimental data, a sen-

Table 3
Predicted values in Newton [N] of the yield load (YL) computed by considering different models. The value in brackets represent the absolute value of the relative error between the numerical and experimental prediction. The benchmark value obtained by in-vitro experimental test [15] is also reported.

		EQB-PD	EQB-CD	EB-PD	EB-CD
ε-based	MPε	3550 (15.4%)	3380 (19.5%)	6566 (56.3%)	5667 (35.0%)
	VMε	4105 (2.3%)	3946 (6.0%)	6656 (58.5%)	6100 (45.2%)
σ-based	MPσ	2042 (51.4%)	2318 (44.8%)	2616 (37.8%)	5513 (31.3%)
	VMσ	2023 (51.8%)	2340 (44.3%)	2476 (41.0%)	5558 (32.3%)
	DPσ	2083 (50.4%)	2490 (40.7%)	2690 (36.0%)	6010 (43.1%)
Exp. YL		4200			

Table 4
Predicted values in Newton [N] of the failure load (FL) computed by considering different models. The value in brackets represent the absolute value of the relative error between the numerical and experimental prediction. The benchmark value obtained by in-vitro experimental test [15] is also reported. Failure mechanisms are also reported in square brackets. SC: Subcapital; TC: Transcervical; TH: Transcapital.

		EQB-PD	EQB-CD	EB-PD	EB-CD
ε-based	MPε	4083 (9.3%) [SC]	3700 (17.8%) [TC]	7695 (71.0%) [SC]	6300 (40.0%) [TC]
	VMε	4567 (1.5%) [SC]	4295 (4.5%) [TC]	8047 (78.8%) [SC]	7063 (57.0%) [TC]
σ-based	MPσ	3537 (21.4%) [TH]	3572 (20.6%) [TC]	4977 (10.6%) [TH]	5577 (23.9%) [TC]
	VMσ	3440 (23.5%) [TH]	3529 (21.6%) [TC]	5008 (11.3%) [TH]	5707 (26.8%) [TC]
	DPσ	3608 (19.8%) [TH]	3667 (18.5%) [TC]	2447 (21.1%) [TH]	6165 (37.0%) [TC]
Exp. FL		4500, SC			

sitivity analysis was performed to assess their impact on the femoral mechanical response, by considering the case of a piecewise-constant description of bone ultimate stress $\sigma_f^{\pm}$ coupled with Drucker-Prager strength criterion (PD-DPσ model). It has been assumed $n_\sigma^+ = n_\sigma^- = n_\sigma$ for duality with the strain-based EQB model, and n_σ is varied with respect to the reference value $n_\sigma = 2$ as shown in Table 5. In the same Table the YL and FL values obtained for the corresponding choice of n_σ are also listed.

The results of the sensitivity analysis are plotted in Fig. 9, and revealed a significant

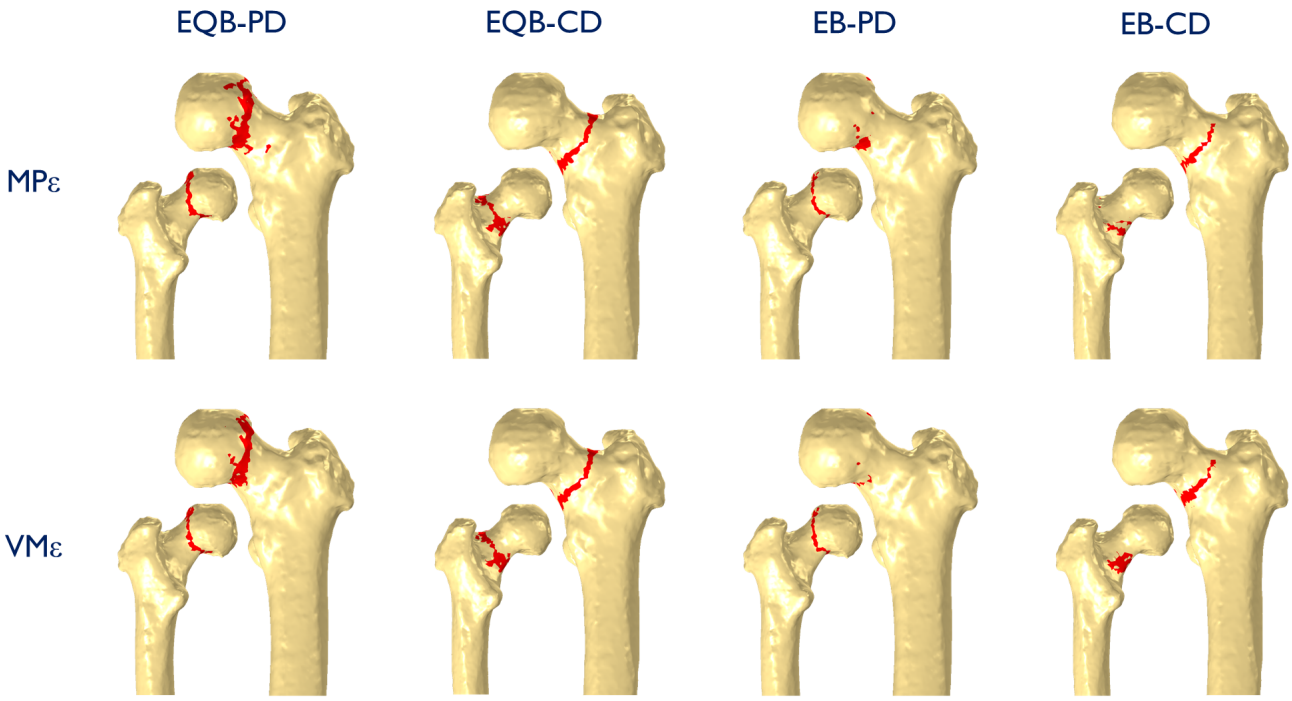

Fig. 5. Damage patterns computed for a boundary displacement value on the top of the femoral head of 2.5 mm for different strain-based damage descriptions. Failure mechanisms are reported in Table 4.

quasi-linear dependence of both YL and FL on the damage-law exponent n_σ (see Fig. 9(b)). In particular, by increasing n_σ, not only the values of YL and FL, but also their difference is found to rise. As a consequence, for higher values of n_σ the progressive failure process of femur results delayed, but also less sudden. Such an occurrence can be related to the fact that an increase in the damage-law exponent reflects into a slower damage propagation, since the ratio $\left(\hat{\varepsilon}/\hat{\varepsilon}_f^{\pm}\right)^{n_\sigma}$ is lower for any fixed $\hat{\varepsilon} < \hat{\varepsilon}_f^{\pm}$ (see Eq. (12)).

Fracture patterns were found to be very similar, and therefore have not been reported for the sake of brevity. It is only remarked that, as just stated, the increase in n_σ induces only a delay in failure onset, but not a different failure mechanism.

4 Discussion

Proposed results show that the constitutive modelling strategy significantly affects the prediction of the overall mechanical behaviour of femur. In fact, the predicted yield (YL) and failure (FL) loads span a wide range of values, as well as considerable variations in post-failure behaviour and the related failure mechanisms are noticed (see Tables 3 and 4). In particular, strain-based formulations seem to be more effective, in agreement with

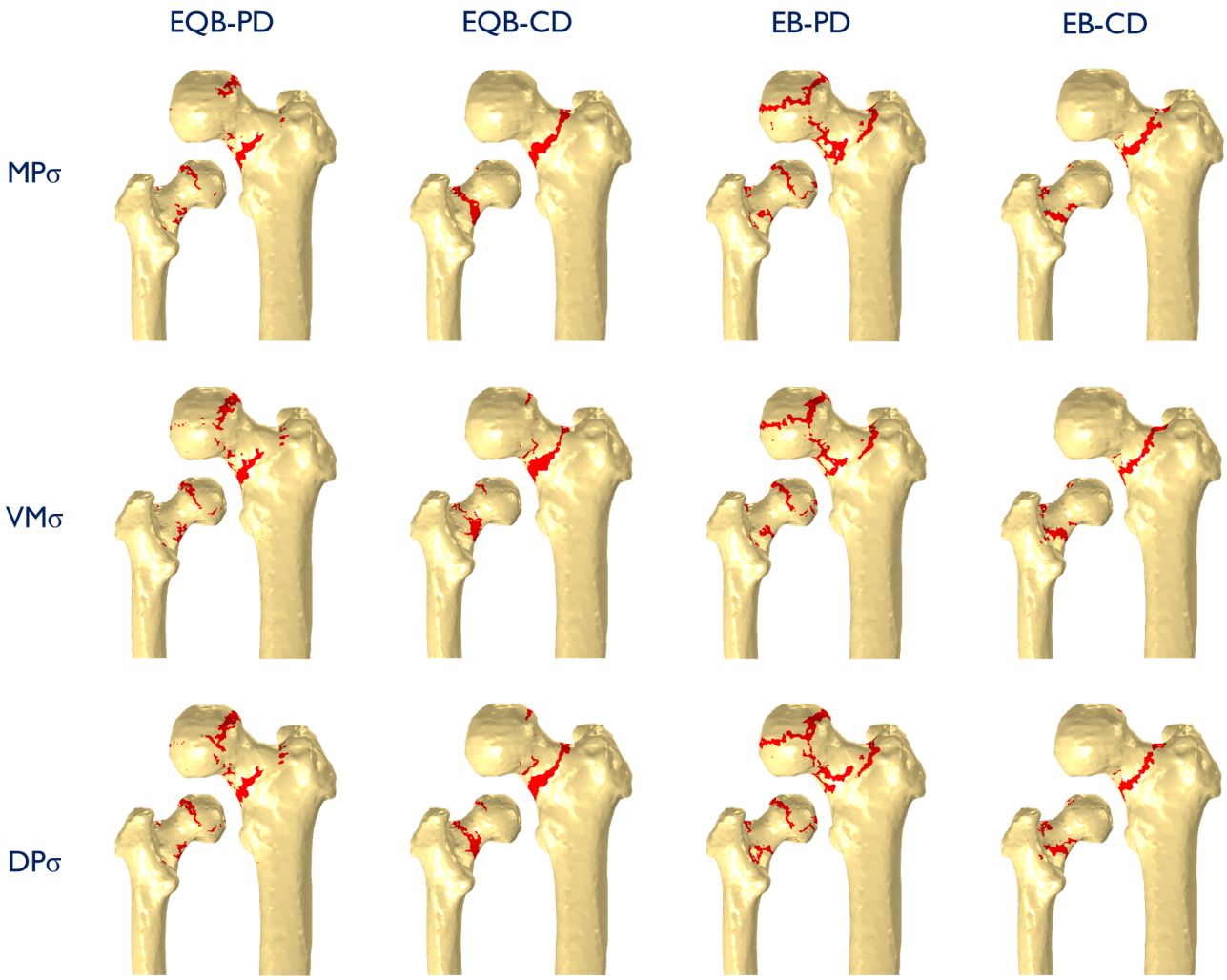

Fig. 6. Damage patterns computed for a boundary displacement value on the top of the femoral head of 2.5 mm for different stress-based damage descriptions. Failure mechanisms are reported in Table 4.

the evidence provided by other authors, supporting the hypothesis that failure process in bony tissues has a strain-driven character [28, 31, 42].

In the framework of strain-based models, the constitutive description of bone as a brittle (EB models) or a quasi-brittle (EQB models) material, significantly affects the mechanical behaviour predicted by numerical simulations. Indeed, EQB strain-based models exhibit a post-failure behaviour characterized by a severe drop in force during the softening phase, in agreement with the characteristic behaviour observed in the experiments [38,60,61]. On the other hand, strain-based EB models overestimate both YL and FL (see Tables 3 and 4), with the worst prediction with respect to the corresponding experimental values achieved by coupling Von Mises strain criterion with a piecewise-constant description of the bone

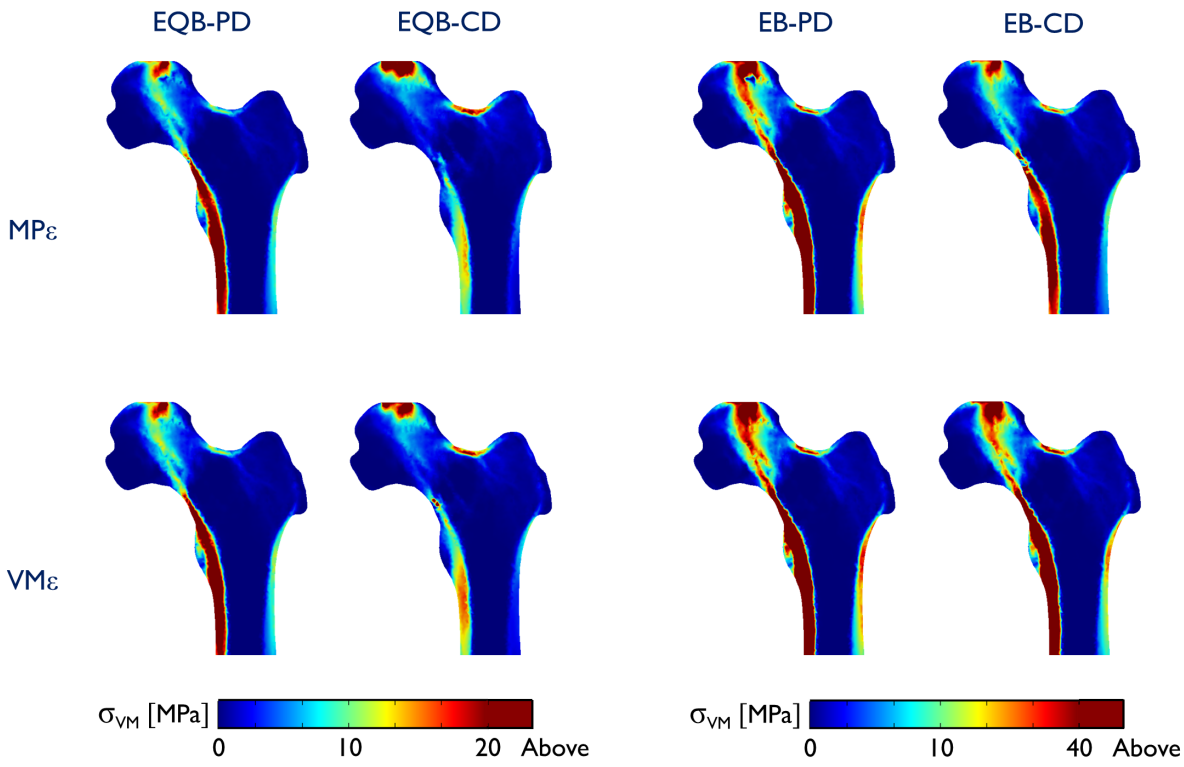

Fig. 7. Distributions of the equivalent Von Mises stress at the coronal section for different damage descriptions defined in terms of strain-based criteria. Results refer to an enforced displacement at the femoral head equal to 1.00 mm and 1.50 mm for EQB and EB models, respectively.

Table 5
Values of the damage law exponent n_σ employed to assess the sensitivity of the stress-based EQB model on the predicted mechanical response. The corresponding values of the Yield Load (YL) and Failure Load (FL) obtained by varying n_σ are also reported.

	Value 1	Value 2	Value 3	Value 4	Value 5
n_σ	2.0 (Reference)	1.0 (-50%)	1.5 (-25%)	2.5 (+25%)	3.0 (+50%)
YL	2083	1496	1752	2451	2792
FL	3608	2044	2714	4490	5440

ultimate strain. Moreover, strain-based EB models exhibit an unrealistic post-yielding branch, characterized by a partial stiffening after the peak load. A significant influence is also revealed by considering different descriptions of the bone strength parameters. In detail, the representation of bone strength parameters via a continuous dependence on the ash density (CD) leads to lower values of YL and FL than a piecewise-constant description (PD). Such an evidence could be explained by the fact that the equation used for strain-based CD models (see Table 1), which is the only relationship actually available to account for a continuous dependence of bone limit strain on the local density, is not accurate,

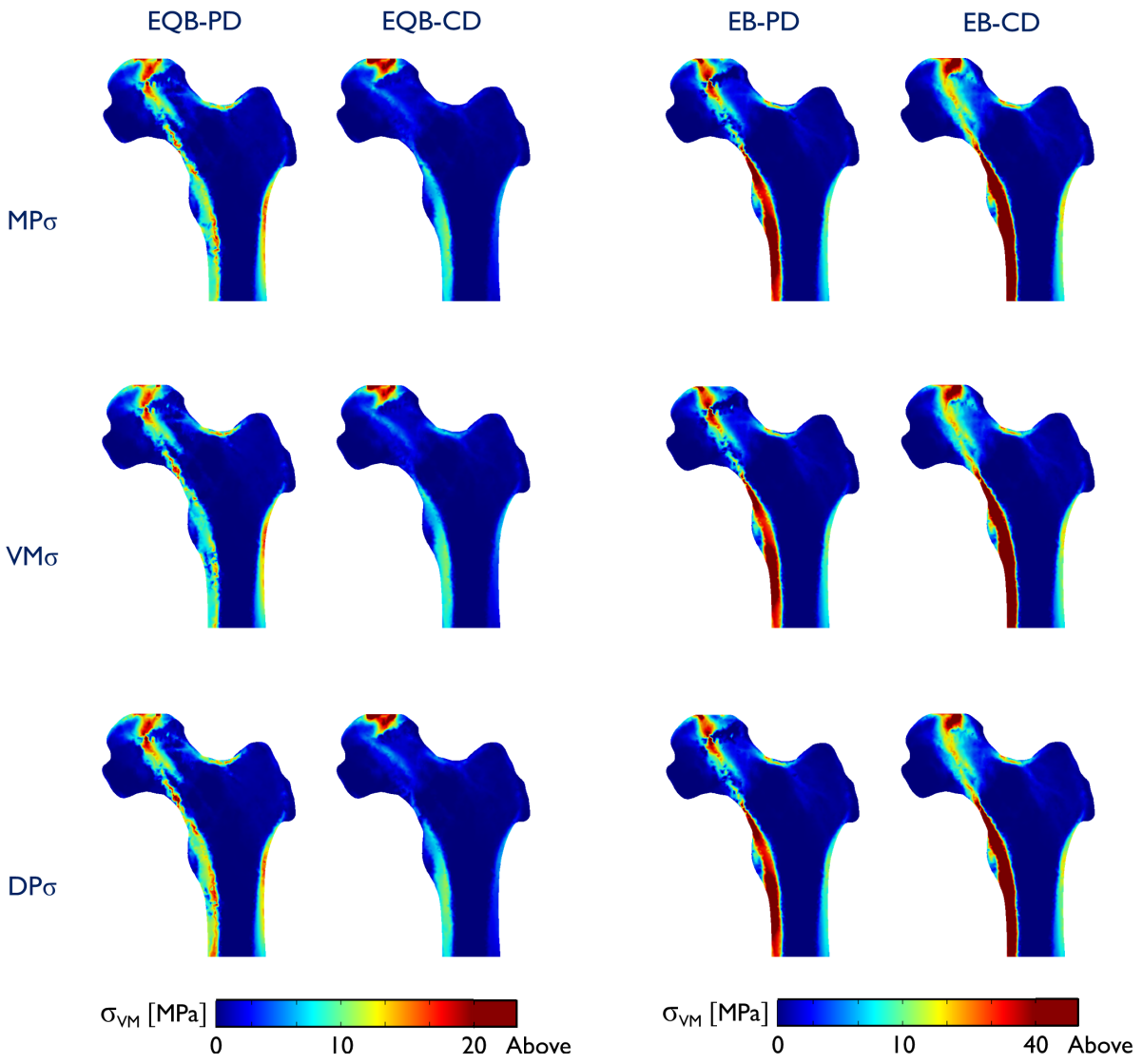

Fig. 8. Distributions of the equivalent Von Mises stress at the coronal section for different damage descriptions defined in terms of stress-based criteria. Results refer to an enforced displacement at the femoral head equal to 1.30 mm and 1.10 mm for EQB and EB models, respectively.

since it was conceived in [50] to describe a yield strain, which is generally lower than the failure one. In addition, failure levels in tensile- and compressive-like states cannot be discriminated. Accordingly, better results with strain-based CD models may possibly be achieved if different relationships, properly set on the basis of the experimental evidence, are employed for describing bone ultimate strain parameters in tension and compression.

Values summarized in Tables 3 and 4 reveal that, for the femur herein investigated, the best agreement with the experimental results is achieved by employing a strain-based approach formulated in terms of Von Mises strength criterion (VMε) and describing a quasi-brittle bone behaviour with piecewise-constant values of the bone ultimate strain

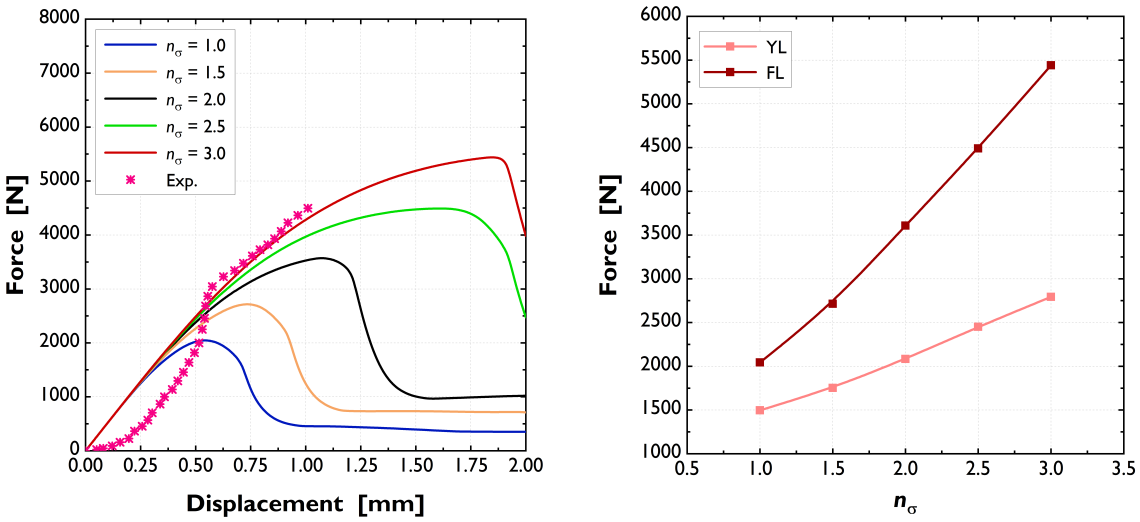

(a) (b)

Fig. 9. Sensitivity analysis with respect to the damage-law exponent n_σ employed in the EQB-PD model based on Drucker-Prager equivalent stress measure. (a) Numerically-experienced force-displacement curves, and (b) variability of the yield load (YL) and failure load (FL) with n_σ. Exp.: experimental data available in [15].

(EQB-PD). Such an approach is able to account for asymmetric bone strength features in tension and compression, and predicted values of YL and FL exhibit relative errors with respect to the experimental data equal to -2.3% and +1.5%, respectively.

As regards stress-based approaches, the EQB description leads to a significant underestimation with respect to the experimental data, partially balanced by considering a brittle behaviour coupled with a continuous description of the bone ultimate parameters (EB-CD). Moreover, as it can be deduced from the plot in the second row of Fig. 4, stress-based models generally predict a lower rate of crack propagation, since the post-yielding behaviour result very prolonged over the displacement range.

The analysis of the onset and evolution of damage patterns highlights that PD strain-based models allow to describe the failure mechanisms of femur herein analyzed in a more faithful way. In detail, with reference to Figs. 5 and 6, and as confirmed by analyzing the stress distributions in Figs. 7 and 8, these models are the only ones able to predict a subcapital fracture, fully in agreement with the in-vitro experimental evidence. In addition, strain-based EQB-PD models properly predict the location of damage onset in the upper neck-head junction region. Specifically referring to the strain-based EQB-PD model formulated by means of VMε strength criterion, Fig. 10 shows the location of the damage onset and the corresponding progressive evolution towards the failure stage. This latter is succesfully compared to the one detected in the experimental test (see Fig. 11), and is mainly characterized by a dominant traction-based damage mechanism in agreement with the experimental evidence [15]. It is worth observing that, although strain-based EB-PD models predict a proper failure mechanism (see Fig. 5), they lead to a delay in the damage

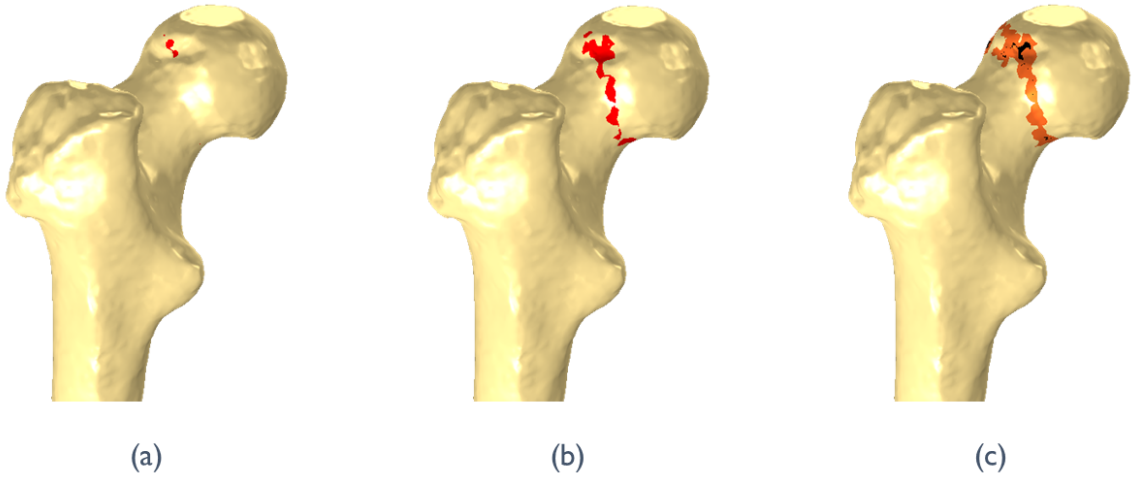

Fig. 10. Strain-based EQB-PD model formulated via the Von Mises strength criterion. (a) Damage initiation, (b) evolution, and (c) failure stage, computed for a displacement at the femoral head respectively equal to 0.80 mm, 1.15 mm and 2.00 mm. In panel (c) elements failed in tension (respectively, compression) are identified by orange (resp., black) colour.

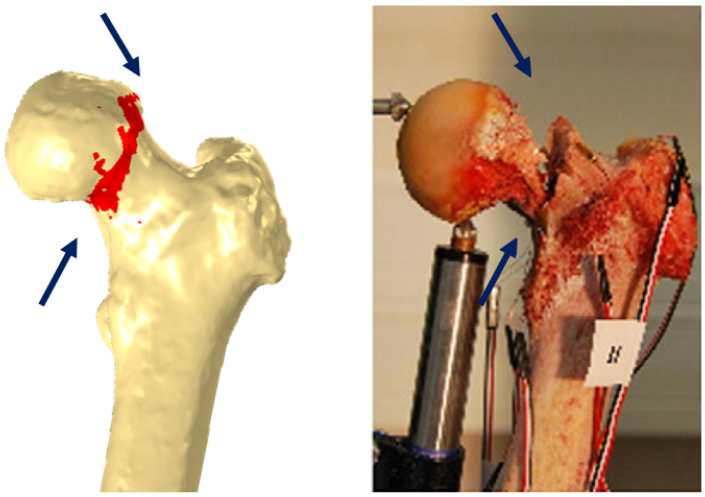

Fig. 11. Comparison between the failure damage pattern predicted by the strain-based EQB-PD model formulated via the Von Mises strength criterion (left) and the failure stage observed during the experimental test [15].

onset and evolution with respect to the strain-based EQB-PD case, resulting in inaccurate values of YL and FL (see Fig. 4).

Concerning the strength criterion, proposed results seem to suggest that its influence on the prediction accuracy of YL and FL is strongly related to its coupling with the damage modelling, and with the description of the bone ultimate parameters. In detail, stress-based approaches have revealed a marginal dependence on the specific strength criterion formulation, whereas more significant effects arise in the case of strain-based models. Moreover, the obtained numerical findings indicate that the particular criterion adopted slightly affects the location of damage onset and failure mechanism, contrarily to the constitutive description.

Although previous results emphasize that, for the femur herein considered, a noticeable accuracy in the prediction of mechanical response can be achieved via a strain-based EQB-PD model, some limitations have to be pointed out. Firstly, present comparative analysis was performed just considering one femur under a stance loading condition. Future work will be focused on analysing a larger cohort, as well as more loading scenarios, such as a sideways fall on the hip. As regards the constitutive description, any fluid and viscous effect has been disregarded, and the hypothesis of an isotropic material symmetry has been assumed. This is clearly an approximation, since many evidence exists in literature showing that bone exhibits an anisotropic behaviour [41, 62]. However, in agreement with other well-established studies [15, 37, 63, 64], the assumption of an isotropic symmetry allows for a simple modelling strategy and it can be retained sufficiently adequate for comparative analyses of femur models under stance loading. On the other hand, it is well-known that bone is a complex material having a nano-micro-macro multiscale hierarchical arrangement of its constitutents, and it exhibits an inhomogeneous porous microstructure [42, 65]. Although material properties are assumed to obey to an inhomogeneous description depending on the local bone density, porous microstructure and multiscale coupled mechanical interactions have been not accounted for. In this framework, possible refinements could be achieved by employing multiscale modelling techniques combined with micro-CT imaging of bone tissue [66], as well as by including dominant patient-specific chemo-mechano-biological mechanisms and fluid-structure interaction effects [67–70].

5 Concluding remarks

In this work, the influence of several modelling approaches on the mechanical response of a femur under a stance loading condition has been numerically assessed. Results obtained by considering different stress- and strain-based failure criteria, combined with two distinct damage evolution laws and two different descriptions of bone ultimate parameters, have been compared to the available experimental data. In particular, the progressive femoral failure has been simulated via a local damage approach, by distinguishing the cases of progressive damage accumulation prior to failure (quasi brittle models) or sudden local rupture (brittle models). Ultimate strain/stress parameters have been considered whether as continuous or piecewise-constant functions of the local bone density.

Starting from computed tomography images of an experimentally-tested cadaveric femur,

computational domain has been reconstructed via a semi-automatic segmentation procedure able to reduce possible partial volume effects. Patient-specific material properties have been derived by the bone density distribution via suitable empirical correlations. The progressive damage process under a stance loading condition has been simulated by means of a finite-element formulation based on a displacement-driven incremental procedure, implemented by accounting for a regularization strategy able to ensure mesh independent results.

Obtained results highlighted that the coupling among the afore-mentioned modelling features significantly affects the global femur mechanical response in terms of damage onset, yield and failure loads, failure mechanism and post-failure behaviour. In particular, for the femur herein studied, the most accurate results have been achieved when a quasi-brittle constitutive response is combined with the strain-based Von Mises strength criterion and with a piecewise-constant dependence of bone ultimate strain on the local density. Such an evidence is in agreement with the hypothesis, previously pointed out by other authors, that femur fracture has a strain-driven character [28, 31, 42].

Accordingly, present study confirms that strain-based failure criteria allow to obtain more accurate predictions than stress-based ones. Nevertheless, a fundamental feature to obtain sound and consistent results is related to the possibility to describe the inhomogeneous and non-symmetric character (with respect to tensile and compressive states) of the material ultimate parameters. In this framework, proposed modelling strategy and discussed results can be considered as a first step towards the development of effective computational tools for the assessment of patient-specific femur fracture risk, useful for supporting the clinical decision-making especially for cases where traditional diagnostic methods are not able to give conclusive indications.

Acknowledgments

Part of this work was carried out within the support from the Italian National Group for Mathematical Physics GNFM-INdAM.

The authors gratefully acknowledge Prof. Zohar Yosibash for providing the experimental data and the CT-scan images of the femur sample herein studied.

Conflict of interests

Pierfrancesco Gaziano, Cristina Falcinelli and Giuseppe Vairo disclose any financial and personal relationships with other people or organizations that could inappropriately influence (bias) their work.

References

[1] I. Fleps, A. Fung, P. Guy, S. J. Ferguson, B. Helgason, P. A. Cripton, Subject-specific ex vivo simulations for hip fracture risk assessment in sideways falls, Bone 125 (2019) 36–45.

[2] S. Haleem, L. Lutchman, R. Mayahi, J. Grice, M. Parker, Mortality following hip fracture: trends and geographical variations over the last 40 years, Injury 39 (10) (2008) 1157–1163.

[3] L. Si, T. Winzenberg, Q. Jiang, M. Chen, A. Palmer, Projection of osteoporosis-related fractures and costs in China: 2010–2050, Osteoporosis International 26 (7) (2015) 1929–1937.

[4] L. J. Melton III, Hip fractures: a worldwide problem today and tomorrow, Bone 14 (1993) 1–8.

[5] P. Garry, M. Edward, R. Setiawati, S. Mustokoweni, F. Mahyudin, Clinical features in metastatic bone disease with and without pathological fractures: A comparative study, Health Notions 3 (10) (2019) 451–459.

[6] Y. Van der Linden, P. Dijkstra, H. Kroon, J. Lok, E. Noordijk, J. Leer, C. Marijnen, Comparative analysis of risk factors for pathological fracture with femoral metastases: results based on a randomised trial of radiotherapy, The Journal of Bone and Joint Surgery. British Volume 86 (4) (2004) 566–573.

[7] W. C. Hayes, E. R. Myers, J. N. Morris, T. N. Gerhart, H. S. Yett, L. A. Lipsitz, Impact near the hip dominates fracture risk in elderly nursing home residents who fall, Calcified Tissue International 52 (3) (1993) 192–198.

[8] T. A. Damron, A. Nazarian, V. Entezari, C. Brown, W. Grant, N. Calderon, D. Zurakowski, R. M. Terek, M. E. Anderson, E. Y. Cheng, et al., CT-based structural rigidity analysis is more accurate than Mirels' scoring for fracture prediction in metastatic femoral lesions, Clinical Orthopaedics and Related Research® 474 (3) (2016) 643–651.

[9] R. F. Mac Niocaill, J. F. Quinlan, R. D. Stapleton, B. Hurson, S. Dudeney, G. C. O'Toole, Inter-and intra-observer variability associated with the use of the Mirels' scoring system for metastatic bone lesions, International Orthopaedics 35 (1) (2011) 83–86.

[10] E. Seeman, P. D. Delmas, Bone quality – The material and structural basis of bone strength and fragility, New England Journal of Medicine 354 (21) (2006) 2250–2261.

[11] K. L. Stone, D. G. Seeley, L.-Y. Lui, J. A. Cauley, K. Ensrud, W. S. Browner, M. C. Nevitt, S. R. Cummings, BMD at multiple sites and risk of fracture of multiple types: long-term results from the study of osteoporotic fractures, Journal of Bone and Mineral Research 18 (11) (2003) 1947–1954.

[12] T. A. Damron, H. Morgan, D. Prakash, W. Grant, J. Aronowitz, J. Heiner, Critical evaluation of Mirels' rating system for impending pathologic fractures, Clinical Orthopaedics and Related Research® 415 (2003) S201–S207.

[13] M. L. Bouxsein, Determinants of skeletal fragility, Best practice & research Clinical rheumatology 19 (6) (2005) 897–911.

[14] F. Eggermont, G. van der Wal, P. Westhoff, A. Laar, M. de Jong, T. Rozema, H. M. Kroon, O. Ayu, L. Derikx, S. Dijkstra, et al., Patient-specific finite element computer models improve fracture risk assessments in cancer patients with femoral bone metastases compared to clinical guidelines, Bone 130 (2020) 115101.

[15] Z. Yosibash, R. Plitman Mayo, G. Dahan, N. Trabelsi, G. Amir, C. Milgrom, Predicting the stiffness and strength of human femurs with real metastatic tumors, Bone 69 (2014) 180–190.

[16] J. Keyak, T. Kaneko, J. Tehranzadeh, H. Skinner, Predicting proximal femoral strength using structural engineering models, Clinical Orthopaedics and Related Research 437 (2005) 219–228.

[17] J. Lotz, E. Cheal, W. C. Hayes, Fracture prediction for the proximal femur using finite element models: part I – linear analysis, journal of Biomechanical Engineering 113 (4) (1991) 353–360.

[18] A. Gustafsson, M. Tognini, F. Bengtsson, T. C. Gasser, H. Isaksson, L. Grassi, Subject-specific fe models of the human femur predict fracture path and bone strength under single-leg-stance loading, Journal of the Mechanical Behavior of Biomedical Materials 113 (2021) 104118.

[19] C. Falcinelli, C. Whyne, Image-based finite-element modeling of the human femur, Computer Methods in Biomechanics and Biomedical Engineering 23 (14) (2020) 1138–1161.

[20] A. Pakdel, J. Fialkov, C. M. Whyne, High resolution bone material property assignment yields robust subject specific finite element models of complex thin bone structures, Journal of biomechanics 49 (9) (2016) 1454–1460.

[21] B. Helgason, E. Perilli, E. Schileo, F. Taddei, S. Brynjólfsson, M. Viceconti, Mathematical relationships between bone density and mechanical properties: A literature review, Clinical Biomechanics 23 (2008) 135–146.

[22] T. Kaneko, M. Pejcic, J. Tehranzadeh, J. Keyak, Relationships between material properties and CT scan data of cortical bone with and without metastatic lesions, Medical Engineering & Physics 25 (2003) 445–454.

[23] T. S. Kaneko, J. S. Bell, M. R. Pejcic, J. Tehranzadeh, J. H. Keyak, Mechanical properties, density and quantitative CT scan data of trabecular bone with and without metastases, Journal of Biomechanics 37 (4) (2004) 523–530.

[24] B. Helgason, S. Gilchrist, O. Ariza, P. Vogt, W. Enns-Bray, R. Widmer, T. Fitze, H. Pálsson, Y. Pauchard, P. Guy, et al., The influence of the modulus–density relationship and the material mapping method on the simulated mechanical response of the proximal femur in side–ways fall loading configuration, Medical Engineering & Physics 38 (7) (2016) 679–689.

[25] J. H. Keyak, S. A. Rossi, Prediction of femoral fracture load using finite element models: an examination of stress–and strain–based failure theories, Journal of Biomechanics 33 (2) (2000) 209–214.

[26] J. H. Keyak, Improved prediction of proximal femoral fracture load using nonlinear finite element models, Medical Engineering & Physics 23 (3) (2001) 165–173.

[27] M. Bessho, I. Ohnishi, J. Matsuyama, T. Matsumoto, K. Imai, K. Nakamura, Prediction of strength and strain of the proximal femur by a CT-based finite element method, Journal of Biomechanics 40 (8) (2007) 1745–1753.

[28] Z. Yosibash, D. Tal, N. Trabelsi, Predicting the yield of the proximal femur using high–order finite–element analysis with inhomogeneous orthotropic material properties, Phil. Trans. R. Soc. A 368 (2010) 2707–2723.

[29] A. Natali, E. Meroi, A review of the biomechanical properties of bone as a material, Journal of Biomedical Engineering 11 (4) (1989) 266–276.

[30] R. K. Nalla, J. H. Kinney, R. O. Ritchie, Mechanistic fracture criteria for the failure of human cortical bone, Nature Materials 2 (3) (2003) 164–168.

[31] R. K. Nalla, J. J. Kruzic, J. H. Kinney, R. O. Ritchie, Mechanistic aspects of fracture and r-curve behavior in human cortical bone, Biomaterials 26 (2) (2005) 217–231.

[32] L. C. Derikx, R. Vis, T. Meinders, N. Verdonschot, E. Tanck, Implementation of asymmetric yielding in case-specific finite element models improves the prediction of femoral fractures, Computer methods in biomechanics and biomedical engineering 14 (02) (2011) 183–193.

[33] D. R. Carter, W. C. Hayes, The compressive behavior of bone as a two–phase porous structure., The Journal of Bone and Joint Surgery. American Volume 59 (7) (1977) 954–962.

[34] T. M. Keaveny, E. F. Wachtel, D. L. Kopperdahl, Mechanical behavior of human trabecular bone after overloading, Journal of Orthopaedic Research 17 (3) (1999) 346–353.

[35] M. Marco, E. Giner, R. Larraínzar-Garijo, J. R. Caeiro, M. H. Miguélez, Numerical modelling of femur fracture and experimental validation using bone simulant, Annals of biomedical engineering 45 (10) (2017) 2395–2408.

[36] R. Hambli, A quasi-brittle continuum damage finite element model of the human proximal femur based on element deletion, Medical & biological engineering & computing 51 (1) (2013) 219–231.

[37] R. Hambli, 3D finite element simulation of human proximal femoral fracture under quasi–static load, Advances in Biomechanics and Applications 1 (2014) 001–014.

[38] R. Hambli, S. Allaoui, A robust 3d finite element simulation of human proximal femur progressive fracture under stance load with experimental validation, Annals of biomedical engineering 41 (12) (2013) 2515–2527.

[39] M. Marco, E. Giner, R. Larraínzar-Garijo, J. R. Caeiro, M. H. Miguélez, Modelling of femur fracture using finite element procedures, Engineering Fracture Mechanics 196 (2018) 157–167.

[40] J. Rittweger, I. Michaeli, M. Giehl, P. Wusecke, D. Felsenberg, Adjusting for the partial volume effect in cortical bone analyses of pqct images, Journal of musculoskeletal and neuronal interactions 4 (4) (2004) 436.

[41] D. C. Wirtz, N. Schiffers, T. Pandorf, K. Radermacher, D. Weichert, R. Forst, Critical evaluation of known bone material properties to realize anisotropic FE–simulation of the proximal femur, Journal of Biomechanics 33 (10) (2000) 1325–1330.

[42] C. Falcinelli, A. Di Martino, A. Gizzi, G. Vairo, V. Denaro, Mechanical behavior of metastatic femurs through patient–specific computational models accounting for bone–metastasis interaction, Journal of the Mechanical Behavior of Biomedical Materials 93 (2019) 9–22.

[43] M. Miura, J. Nakamura, Y. Matsuura, Y. Wako, T. Suzuki, S. Hagiwara, S. Orita, K. Inage, Y. Kawarai, M. Sugano, N. K., S. Ohtori, Prediction of fracture load and stiffness of the proximal femur by CT–based specimen specific finite element analysis: cadaveric validation study, BMC Musculoskeletal Disorders 18 (2017) 1–8.

[44] M. Goodsitt, Conversion relations for quantitative bone mineral densities measured with solid and liquid calibration standards, Bone and Mineral 19 (1992) 145–158.

[45] D. Kondo, H. Welemane, F. Cormery, Basic concepts and models in continuum damage mechanics, Revue européenne de génie civil 11 (7-8) (2007) 927–943.

[46] J. C. Simo, J. Ju, Strain– and stress–based continuum damage models – I. Formulation, International Journal of Solids and Structures 23 (7) (1987) 821–840.

[47] J. Lemaitre, A continuous damage mechanics model for ductile fracture.

[48] T. Arthur Moore, L. Gibson, Microdamage accumulation in bovine trabecular in uniaxial compression, Journal of Biomaterials 124 (2002) 63–71.

[49] U. Wolfram, H.-J. Wilke, P. K. Zysset, Damage accumulation in vertebral trabecular bone depends on loading mode and direction, Journal of Biomechanics 44 (6) (2011) 1164–1169.

[50] D. Dragomir-Daescu, J. Op Den Bujis, S. McEligot, Y. Dai, R. Entwistle, C. Salas, K. Bennet, Robust QCT/FEA models of proximal femur stiffness and fracture load during a sideways fall on the hip, Ann Biomed Eng 1 (2011) 742–755.

[51] T. Keller, Predicting the compressive mechanical behavior of bone, Journal of Biomechanics 27 (1994) 1159–1168.

[52] J. Keyak, I. Lee, H. Skinner, Correlations between orthogonal mechanical properties and density of trabecular bone: use of different densitometric measures, Journal of biomedical materials research 28 (11) (1994) 1329–1336.

[53] A. S. Khan, S. Huang, Continuum theory of plasticity, John Wiley & Sons, 1995.

[54] G. Pijaudier-Cabot, Z. P. Bažant, Nonlocal damage theory, Journal of Engineering Mechanics 113 (10) (1987) 1512–1533.

[55] W. Brekelmans, J. De Vree, Reduction of mesh sensitivity in continuum damage mechanics, Acta Mechanica 110 (1) (1995) 49–56.

[56] D. Zuo, S. Avril, C. Ran, H. Yang, S. J. Mousavi, K. Hackl, Y. He, Sensitivity analysis of non-local damage in soft biological tissues, International Journal for Numerical Methods in Biomedical Engineering 37 (3) (2021) e3427.

[57] D. Zuo, S. Avril, H. Yang, S. J. Mousavi, K. Hackl, Y. He, Three-dimensional numerical simulation of soft-tissue wound healing using constrained-mixture anisotropic hyperelasticity and gradient-enhanced damage mechanics, Journal of the Royal Society Interface 17 (162) (2020) 20190708.

[58] I. H. Parkinson, N. L. Fazzalari, Interrelationships between structural parameters of cancellous bone reveal accelerated structural change at low bone volume, Journal of Bone and Mineral Research 18 (12) (2003) 2200–2205.

[59] C. Pattin, W. Caler, D. Carter, Cyclic mechanical property degradation during fatigue loading of cortical bone, Journal of Biomechanics 29 (1996) 69–79.

[60] L. Grassi, S. P. Väänänen, S. Amin Yavari, J. S. Jurvelin, H. Weinans, M. Ristinmaa, A. A. Zadpoor, H. Isaksson, Full-field strain measurement during mechanical testing of the human femur at physiologically relevant strain rates, Journal of biomechanical engineering 136 (11) (2014) 111010.

[61] M. Marco, E. Giner, J. R. Caeiro-Rey, M. H. Miguélez, R. Larraínzar-Garijo, Numerical modelling of hip fracture patterns in human femur, Computer methods and programs in biomedicine 173 (2019) 67–75.

[62] G. Yang, J. Kabel, B. Van Rietbergen, A. Odgaard, R. Huiskes, S. C. Cown, The anisotropic hooke's law for cancellous bone and wood, Journal of Elasticity 53 (2) (1998) 125–146.

[63] L. Peng, J. Bai, X. Zeng, Y. Zhou, Comparison of isotropic and orthotropic material property assignments on femoral finite element models under two loading conditions, Medical Engineering & Physics 28 (3) (2006) 227–233.

[64] W. S. Enns-Bray, J. S. Owoc, K. K. Nishiyama, S. K. Boyd, Mapping anisotropy of the proximal femur for enhanced image based finite element analysis, Journal of Biomechanics 47 (13) (2014) 3272–3278.

[65] C. Falcinelli, A. Di Martino, A. Gizzi, G. Vairo, V. Denaro, Fracture risk assessment in metastatic femurs: a patient-specific ct-based finite-element approach, Meccanica 55 (4) (2020) 861–881.

[66] A. A. Poundarik, D. Vashishth, Multiscale imaging of bone microdamage, Connective Tissue Research 56 (2) (2015) 87–98.

[67] D. Bianchi, M. Marino, G. Vairo, An integrated computational approach for aortic mechanics including geometric, histological and chemico-physical data, Journal of biomechanics 49 (12) (2016) 2331–2340.

[68] M. Vasta, A. Gizzi, A. Pandolfi, On three-and two-dimensional fiber distributed models of biological tissues, Probabilistic Engineering Mechanics 37 (2014) 170–179.

[69] M. Marino, G. Pontrelli, G. Vairo, P. Wriggers, A chemo-mechano-biological formulation for the effects of biochemical alterations on arterial mechanics: the role of molecular transport and multiscale tissue remodelling, Journal of The Royal Society Interface 14 (136) (2017) 20170615.

[70] M. Vasta, A. Gizzi, A. Pandolfi, A spectral decomposition approach for the mechanical statistical characterization of distributed fiber-reinforced tissues, International Journal of Non-Linear Mechanics 106 (2018) 258–265.

Conflict of Interest (Please upload in word format)

Declaration of interests

☒The authors declare that they have no known competing financial interests or personal relationships that could have appeared to influence the work reported in this paper.

☐The authors declare the following financial interests/personal relationships which may be considered as potential competing interests:

Author Agreement

Title of the manuscript: A computational insight on damage-based constitutive modelling in femur mechanics
Authors: Pierfrancesco Gaziano, Cristina Falcinelli, Giuseppe Vairo
Submitted to European Journal of Mechanics - A/Solids

The undersigned authors hereby declare that this is an original paper which has neither previously, nor simultaneously, in whole or in part, been submitted anywhere else.

We wish to confirm that there are no known conflicts of interest associated with this publication and there has been no financial support, personal or other relationships with other people or organizations that could inappropriately influence, or be perceived to influence, this work.

We confirm that the submitted manuscript has been read and approved by all named authors and that there are no other persons who satisfied the criteria for authorship but are not listed. We further confirm that the order of authors listed in the manuscript has been approved by all of us.

Each author declares to have materially participated to the research effort and to the article preparation.

Pierfrancesco Gaziano, Cristina Falcinelli, Giuseppe Vairo